Human Brain Mapping

WILEY

RESEARCH ARTICLE OPEN ACCESS

Regional Changes in the Fetal Telencephalic Wall Diffusion Metrics Across Late Second and Third Trimesters

Camilo Calixto[1,2,3] | Maria C. Cortes-Albornoz[1,2,4] | Clemente Velasco-Annis[1,2] | Davood Karimi[1,2] | Onur Afacan[1,2] | Simon K. Warfield[1,2] | Ali Gholipour[1,2,5] | Camilo Jaimes[1,4]

[1]Harvard Medical School, Boston, Massachusetts, USA | [2]Computational Radiology Laboratory. Department of Radiology, Boston Children's Hospital, Boston, Massachusetts, USA | [3]Icahn School of Medicine at Mount Sinai, New York City, New York, USA | [4]Massachusetts General Hospital, Boston, Massachusetts, USA | [5]Department of Radiological Sciences, University of California Irvine, Irvine, California, USA

Correspondence: Camilo Jaimes (cjaimescobos@mgb.org)

Received: 1 April 2024 | **Revised:** 28 January 2025 | **Accepted:** 30 January 2025

Funding: This work was supported by American Roentgen Ray Society. Rosamund Stone Zander Translational Neuroscience Center at Boston Children's Hospital. Office of Faculty Development at Boston Children's Hospital. Eunice Kennedy Shriver National Institute of Child Health and Human Development, R01 HD109395, R01 HD110772. National Institute of Neurological Disorders and Stroke, R01 NS106030, R01 NS121657, R01 NS128281. NIH Office of the Director, S10 OD0250111. National Institute of Biomedical Imaging and Bioengineering, R01 EB013248, R01 EB031849, R01 EB032366, R01EB018988.

ABSTRACT

During the second and third trimesters of human gestation, the brain undergoes rapid neurodevelopment thanks to critical processes such as neuronal migration, radial glial scaffolding, and synaptic sprouting. Unfortunately, gathering high-quality MRI data on the healthy fetal brain is complex, making it challenging to understand this development. To address this issue, we conducted a study using motion-corrected diffusion tensor imaging (DTI) to analyze changes in the cortical gray matter (CP) and sub-cortical white matter (scWM) microstructure in 44 healthy fetuses between 23 and 36 weeks of gestational age. We automatically segmented these two tissues and parcellated them into eight regions based on anatomy, including the frontal, parietal, occipital, and temporal lobes, cingulate, sensory and motor cortices, and the insula. We were able to observe distinct patterns of diffusion MRI signals across these regions. Specifically, we found that in the CP, fractional anisotropy (FA) consistently decreased with age, while mean diffusivity (MD) followed a downward-open parabolic trend. Conversely, in the scWM, FA exhibited an upward-open parabolic trajectory, while MD followed a downward-open parabolic trend. Our study underscores the potential for diffusion as a biomarker for normal and abnormal neurodevelopment before birth, especially since most neurodiagnostic tools are not yet available at this stage.

1 | Introduction

During fetal development, a highly regulated series of cellular and molecular processes are responsible for the formation of the human cerebral cortex. Neuronal progenitors from the ventricular and subventricular zones migrate toward the cortical plate (CP), creating the mature, multi-layered structure of the cortex (Rakic 1995). Inhibitory interneurons, on the other hand, emerge from the ganglionic eminence and migrate tangentially toward their cortical targets (Pleasure et al. 2000). The subplate (SP) is also instrumental in facilitating neuronal migration, early synapse formation, and axonal guidance (Ohtaka-Maruyama 2020). Our current understanding of these mechanisms is based mainly on animal studies and molecular biology assays involving tissue samples. The challenges associated with studying these processes in utero, with sufficient spatial resolution and biological specificity, have limited our ability to translate this knowledge to clinical practice.

Fetal MRI has emerged as a valuable technique in fetal neurology and fetal neuroscience. The versatility of MRI as an imaging modality, coupled with its high spatiotemporal resolution

Summary

- By employing advanced diffusion tensor imaging motion correction techniques and automatic segmentation in the diffusion space, this study reveals the dynamic changes in water diffusivity and anisotropy within the fetal telencephalic wall.
- These changes are closely linked to critical developmental processes such as neuronal migration and synaptic formation.
- The findings offer crucial insights into the prenatal onset of brain region specialization and provide a foundation for identifying normal and abnormal brain development markers.
- This work offers a new perspective on early brain maturation and its implications for assessing normal maturation.

and advantageous safety profile (Chartier et al. 2019; Jaimes et al. 2019), offers the prospect of vastly expanding our ability to study human brain development in utero safely. Advances in computational neuroimaging have further closed this gap by mitigating the artifacts related to fetal motion, B0, and B1 inhomogeneities and enabling quantitative analyses (Afacan et al. 2019). This emerging technology has opened new possibilities for studying volumetric growth, functional connectivity (Taymourtash et al. 2022), structural connectivity (Marami et al. 2017), and microstructure (Calixto et al. 2023a), which were previously unattainable.

The advances in image processing have been particularly beneficial for diffusion MRI of the fetal brain (Marami et al. 2016). Postnatally, diffusion MRI has a strong track record as a robust tool for investigating microstructure, and therefore, it holds great potential for investigating the complex developmental process of the fetal brain (Kunz et al. 2014). The existing body of research is largely limited to ex vivo studies or premature infants (Maas et al. 2004; McKinstry 2002). Trivedi and colleagues conducted microstructural analyses on 50 preserved fetal brains and identified region-specific changes (Trivedi et al. 2009). Ball et al. and Ouyang et al. also conducted microstructural analyses on the cortex of pre-term infants, and in addition to identifying region-specific changes, they observed significant effects resulting from prematurity (Ball et al. 2015; Ouyang et al. 2019). More recently, Calixto et al. utilized motion-robust fetal brain DTI to create nomograms of microstructural change across various regions of the fetal brain (Calixto et al. 2023a). While this work presented stereotypical patterns of gestational-age-related changes across the entire CP, it did not specifically evaluate regional trends.

The objective of this research is to examine the diversity in cortical microstructure among eight distinct regions in the cortical plate (CP) and subcortical white matter (scWM) of healthy fetuses aged between 23 and 36 weeks of GA. We hypothesize that, despite the neocortex's uniform layered architecture and shared cell population, differences in cortical regions during fetal development will be discernible using cutting-edge computational neuroimaging techniques, including motion-corrected fetal brain DTI.

2 | Materials and Methods

2.1 | Subjects

This study used data from in utero fetal MRI scans conducted as part of a prospective research study at Boston Children's Hospital (BCH) in Boston, MA, from March 2013 to May 2019. The study followed HIPAA guidelines and was approved by the BCH Institutional Review Board (IRB). All participants provided written informed consent before each fetal MRI examination. The study was promoted through brochures at outpatient obstetrics and gynecology clinics, at our institution, and banners on the hospital's intranet.

The inclusion criteria were mothers between 18 and 45 years old with normal pregnancies and gestational age (GA) between 23 and 36 weeks, which was determined based on the routine first-trimester ultrasound. The exclusion criteria were any contraindications to MRI, high-risk pregnancy (including patients with hypertension, diabetes, overweight/obesity, multiple pregnancies, chronic kidney disease, or requiring any medication for medical management), fetal anomalies (e.g., congenital heart disease, diaphragmatic hernia, or brain anomalies) as identified by a second-trimester ultrasound, and substance abuse (assessed during the pre-scan interview with yes/no questions about tobacco, alcohol [during pregnancy], marijuana, cocaine, and amphetamines).

2.2 | MRI Data Acquisition Protocol

The MRI scans were conducted in 3.0 T scanners (Skyra and Prisma, Siemens Medical Solutions in Erlangen, Germany). The scanners were equipped with a 16-channel body array and spine coils. The dimensions of the maternal and fetal subjects determined the field of view (FOV) and the number of slices captured. No sedation was used for any of the women imaged.

Multiple T2-weighted Half-Fourier Single Shot Turbo Spin Echo (HASTE) sequences were prescribed in each orthogonal plane (axial, coronal, and sagittal) of the fetal brain for structural fetal brain MRI. Acquisition parameters were: TR of 1400–2000 ms, TE of 100–120 ms, in-plane resolution of 0.9–1.1 mm, and slice thickness of 2 mm with no inter-slice space.

For diffusion-weighted images (DWI), 2–8 scans were taken, each along one of the orthogonal planes relative to the fetal head. For each scan, one or two $b = 0\,s/mm^2$ images and 12 diffusion-sensitized images at $b = 500\,s/mm^2$ were obtained. The acquisition parameters were: TR of 3000–4000 ms, TE of 60 ms, in-plane resolution of 2 mm, and slice thickness of 2–4 mm.

2.3 | Image Processing

Image processing involved three main components: (1) reconstructing an isotropic-resolution T2w volume for each fetal brain through motion-robust super-resolution volume reconstruction from slice acquisitions (Gholipour, Estroff, and

Warfield 2010; Kainz et al. 2015); (2) fitting a diffusion tensor imaging (DTI) model for each fetal brain using a motion-tracking based slice-to-volume registration and robust DTI reconstruction algorithm (Marami et al. 2017); and (3) registering the reconstructed T2w and DTI images to standard spatiotemporal fetal brain MRI atlases followed by atlas-based segmentation (Gholipour et al. 2017; Khan et al. 2019). We provide a brief overview of each component below; however, for full details of each algorithm, we refer to the corresponding papers cited above. Specifically, for fetal brain DTI reconstruction, we refer to (Marami et al. 2017).

To reconstruct a T2w isotropic structural image, a slice-to-volume registration approach is used in an iterative model-based super-resolution framework. This framework realigns T2w slices, rejects motion-corrupted slices, reconstructs a volume by solving an inverse problem that minimizes a data consistency term for all of the realigned slices, and repeats this process using the reconstructed volume as reference for the next iteration of slice realignment. Through a few iterations, both slice realignment and super-resolution reconstruction are improved, and a T2w isotropic structural image is reconstructed. The details of this algorithm can be found in a series of publications (Gholipour, Estroff, and Warfield 2010; Kainz et al. 2015; Kuklisova-Murgasova et al. 2012). Following the procedure outlined by Gholipour et al., the reconstructed image is then brain-extracted, bias-corrected, registered to a standard atlas space, and segmented to brain tissue and regions (Gholipour et al. 2017).

We then screened available studies to ensure that at least two DWI scans were of sufficient quality for successful DTI reconstruction and registration to structural T2-weighted scans. Fetal DTI reconstruction was performed using the method developed and described by Marami et al. 2017. This method has two core components: (1) motion-tracking-based slice-to-volume registration for fetal DWI and (2) robust DTI reconstruction from motion-corrected slices. The first component involved dynamic motion correction using a new temporal slice-to-volume registration reinforced with Kalman smoothing with a temporal window of five slices. While DWI slice-to-volume registration is challenged by the relatively low signal-to-noise ratio and the varying contrast due to different diffusion sensitization across volumes, the state space estimation with Kalman smoothing proposed in (Marami et al. 2017) regulated the slice-to-volume registration. Based on transformations obtained per slice from the first component, a variable-length data structure was created for each voxel of the fetal brain on a target isotropic-resolution 3D image grid for DTI reconstruction. This data structure involved any number of DWI measurements in the vicinity of a target voxel on the grid, along with the b value, gradient direction (corrected with the slice transformations), and a kernel weight corresponding to that measurement that was based on the distance of the mapped slice voxel to the target voxel. A DTI model was then fit at every target voxel using constrained weighted linear least squares (CWLLS) that took into account the kernel weight of every measurement. For the details of this algorithm and calculations, we refer to Marami et al. (Marami et al. 2017). All DTI-derived scalars, including fractional anisotropy (FA) and mean diffusivity (MD), were calculated from the reconstructed DTI. It is noteworthy that this algorithm directly reconstructs DTIs aligned with the reconstructed T2w images of the fetus. To achieve this, the algorithm constructs composite $b = 0$ and $b \neq 0$ at the beginning that are registered to each other and to the reconstructed T2w image of the fetus. The composite diffusion-sensitized image ($b \neq 0$) is then used as the reference for motion tracking based slice to volume registration, and the composite $b = 0$ image is used as the reference signal in DTI model fitting.

The reconstructed images were then examined for the presence of gross reconstruction errors, insufficient visibility of brain structures, or erroneous direction of the principal eigenvectors and were rated on a scale of 1–4, where 1 is a good reconstruction, and 4 is where data is not usable. Only images rated 1 or 2 were used. A detailed description of the criteria used for image rating can be found in Table S1, and example images for each grading can be found in Figure S1.

2.4 | Image Segmentation

We used a multiple-template-based framework to automatically segment the fetal cortical plate (CP) and subcortical white matter (scWM). The framework utilized templates from an annotated fetal brain DTI atlas (Calixto et al. 2023b) and 14 manually annotated individual fetuses. The atlas spawned the period between 23 and 36 weeks after conception, while the individual subjects were evenly distributed across this same range of gestational ages—one subject per week of postconceptional age. The segmentations contained labels for CP and scWM, parcellated to the frontal, parietal, temporal, and occipital lobes, as well as the insula, cingulum, and motor and sensory cortices. Of note, we opted not to include a parcellation for the insular scWM. The reason for this is that delineating the boundaries of this area, which corresponds to the extreme capsule, is challenging due to the partial volume averaging between the gray matter of the putamen, claustrum, and insula.

Two research fellows (omitted for peer review, MD and omitted for peer review, MD) performed the segmentations of the individual subjects, following the same procedure used in the atlas segmentations as described by Calixto et al. (Calixto et al. 2023b). These segmentations were then reviewed and revised as needed by a board-certified neuroradiologist with fellowship training in pediatric neuroradiology (omitted for peer review, MD, who has 6 years of experience in fetal imaging). The segmentation process was carried out using high-resolution (1080p) Wacom Cintiq tablets and ITK-SNAP (version 4.0.1).

2.4.1 | Label Propagation

To carry out label propagation, we used the tensor-based deformable registration algorithm in DTI-TK to register the DTI atlases and manually segmented diffusion images closest to a subject's gestational age (t-1, t, and $t+1$; where "t" is in weeks), to the DTI map of the subject. This ensured that every subject had between 4 and 6 prior segmentations. Then multiple-template-based segmentation was carried out using probabilistic STAPLE. We excluded automatic segmentations with significant errors, and we

ensured the accuracy of the remaining segmentations by having an expert carry out a manual refinement.

2.5 | Statistical Analysis

We calculated median FA and MD values for each subject in each ROI. To assess changes in FA and MD throughout gestation, we used mixed-effects models with subject ID as a random effect to account for repeated measurements due to ROIs being present in both hemispheres. We evaluated two different models for each combination of ROI and diffusion metric based on previously described trajectories of DTI-derived metrics (Machado-Rivas et al. 2021): a quadratic model:$\text{medianValue}^{\text{Predicted}}(\text{GA}) = \text{a} + \text{b} \times \text{GA} + \text{c} \times \text{GA}^2$, where GA is the gestational age in weeks, a is the intercept, b is the week coefficient, and c is the coefficient of the quadratic week term; and an exponential decay model: $\text{medianValue}^{\text{Predicted}}(\text{GA}) = \text{Asym} + (\text{R0} - \text{Asym})e^{-e^{\text{lrc}} \times \text{GA}}$, where Asym is the horizontal asymptote on the right side, R0 is the response when week = 0, and lrc is the natural logarithm of the rate constant. After fitting the two models, Akaike Information Criteria (AIC) was used for model selection.

We depicted changes over gestation with different estimates depending on the model type. For structures that followed an exponential decay model, we used the decay constant to portray the speed with which changes occur. For structures that followed a parabolic trend, we defined a turning point—which corresponds to the vertex of the parabola—to assess the time in gestation when a change in trend occurred.

We used a wild bootstrapping scheme to calculate accurate confidence intervals for the decay constants and vertices of the parabolas (Dikta and Scheer 2021). Our process involved fitting a quadratic or exponential model, and then computing a new Y^* based on: $y_i^* = \hat{y}_i + \hat{\varepsilon}_i v_i$ (where $\hat{y}$ is the predicted value, $\hat{\varepsilon}$ is the estimated residual and v_i is a random variable which comes from a Rademacher distribution) for each bootstrap sample. We utilized the new Y^* to fit a new model and estimate the vertex of the parabola or decay constant. This process was repeated 10,000 times, and the resulting distribution of estimates was used to calculate 95% confidence intervals.

In order to analyze the rate of change for each curve at any given point and be able to compare them between other cortical or subcortical parcellations and the two diffusion metrics, we applied the previous models to z-normalized data and subsequently determined their derivatives.

2.5.1 | Hemispheric Asymmetries

We analyzed hemispheric asymmetry by using the laterality index, represented as LI, for each ROI (X). LI of X was calculated as: $LI(X) = 100 \times \frac{X_R - X_L}{X_R + X_L}$, where X_R and X_L are the diffusivity values (either FA or MD) of the right and left ROIs, respectively. A positive $LI(X)$ value indicates rightward asymmetry, and a negative value suggests leftward asymmetry. A one-sample, two-tailed t-test was used to examine whether there was asymmetry ($LI \neq 0$) in terms of X across GA. Additionally, with no significant asymmetry, we analyzed the relationship between LI versus GA using linear regression to see if the lack of significance was due to changes in asymmetry with increasing age. An ROI with a positive significant slope is said to have a changing asymmetry from left to right, while a negative slope would mean changing asymmetry from right to left.

All calculations were completed in R (version 4.2.3) (R Core Team 2023), using a significance level of 0.05. We calculated mixed-effects models using the lmerTest (version 4.1–3) (Kuznetsova, Brockhoff, and Christensen 2017) and nlme (version 3.1–162) (Pinheiro et al. 2023) packages. To control the family-wise error rate when conducting multiple statistical tests, we performed Holm–Bonferroni correction for multiple comparisons at an α of 0.05. Plots were designed using the ggplot2 package (version 3.4.1) (Wickham 2016).

To better assess changes in water diffusion in each ROI throughout gestation, we depicted diffusion tensors using glyphs. We calculated median eigenvalues (λ_1, λ_2 and λ_3) for each ROI at every gestational age, and then generated a visualization for each "average" tensor using superquadric surfaces as defined by Kindlmann (Ennis et al. 2005; Kindlmann 2004). Superquadric surfaces were chosen over the typical ellipsoids, which can exhibit visual similarities from certain perspectives due to their shared profiles and shading characteristics. On the other hand, superquadric glyphs provide a more precise visualization and offer the flexibility to illustrate transitions between different tensor shapes, such as linear to planar anisotropy.

3 | Results

3.1 | Study Sample Characteristics

We conducted scans on 86 pregnant women, with some being scanned at two different times during pregnancy, resulting in 101 fetal diffusion MRI scans. Of these, 37 were excluded due to poor post-reconstruction data. Additionally, 20 were excluded due to gross segmentation errors. After this, our study sample consisted of 44 fetal diffusion MRI scans from 44 distinct fetuses. Table 1 displays information about the pregnant volunteers and the analyzed fetal cohort, and Table S2 shows this information stratified by GA.

3.2 | Diffusion Analysis

We observed significant age-related changes in all ROIs ($p < 0.05$), as illustrated in Figures 1 and 2. There were no significant differences between the left and right hemispheres for any ROIs in the two diffusion metrics ($p > 0.5$).

3.2.1 | Cortical Plate

FA in the CP followed an exponential decay trend, with the sensorimotor regions exhibiting the fastest changes (Table 2, Figure 1), followed by the cingulum and frontal and occipital lobes, and finally, the parietal and temporal association regions.

TABLE 1 | Study sample characteristics.

Group and characteristic	Number of individuals (%)
Pregnant volunteers	44
Age[a]	32.1 [30.1–34.4]
Number of volunteers with data for self-described race	35
Asian	3 (6.8%)
Black or African American	2 (4.5%)
White	30 (68%)
Number of volunteers with data for self-described ethnicity	35
Hispanic	2 (4.5%)
Non-Hispanic	33 (75%)
Number of fetuses	44
Gestational age[a]	29.1 [26.6–32.3]
Number of MRI examinations corresponding to fetuses < 31 weeks of gestational age	29 (65.9%)
Sex	
Female	15 (34%)
Male	29 (66%)

[a]Data are median (interquartile range).

By the end of our study period, the frontal lobe had the highest FA, while the occipital lobe had the lowest.

In contrast, MD trends in the CP followed a downward-opened parabolic pattern. Most CP parcellations reached their peak MD between 23.3 and 29.3 weeks of gestation, with the sensorimotor areas peaking earlier, followed by the occipital, and parietal and temporal association areas. The frontal region and the cingulate cortex were the last to reach their peak. At the end of our study period, the sensorimotor area had the lowest MD, while the occipital lobe had the highest.

3.2.2 | Subcortical White Matter

In the scWM, FA followed an upward-open parabolic pattern, with all parcellations reaching their minimum point of FA between 31.1 and 32.8 weeks of gestation (Table 3). The sensorimotor areas displayed the fastest changes in FA, whereas the temporal and parietal association areas exhibited the slowest changes (Figure 2). Among all areas, the sensorimotor region was the first to reach its minimum point, and the parietal, occipital, and frontal regions were the last. By the end of our study period, the sensorimotor areas had the highest FA, while the occipital lobe had the lowest.

Conversely, trends of MD followed a downward-opened parabolic pattern, with all scWM parcellations reaching their maximum point of MD between 25.1 and 29.3 weeks of gestation. The occipital lobe showed the fastest changes in MD, while the sensory area exhibited the slowest changes (Figure 3). In a similar vein, the sensorimotor area was the first to reach its maximum peak in MD, while the occipital was the latest. By the end of our study period, the occipital lobe had the highest FA, while the sensorimotor areas had the lowest.

3.2.3 | Insula

The insula exhibited the most rapid changes in FA among all the CP parcellations. However, the initial FA values were slightly lower than those of the other cortical parcellations, with an average difference of 0.07 units. Moreover, the insula's MD peaked before the scope of our study, at approximately 18.1 weeks of gestation, and showed a consistent decrease throughout the study period. While the insula's initial MD values were, on average, 0.1 mm^2/s higher than its counterparts, it ultimately ended at an average similar to the others.

4 | Discussion

Our research utilized motion-corrected DTI to investigate the spatiotemporal evolution of cortical diffusivity and anisotropy in live human fetuses as surrogates for microstructural maturation. We observed rapid evolution in diffusion MRI signals in the CP and scWM, with distinct speeds and trajectories across anatomy-derived parcels. In the CP, FA consistently decreased with age, while MD followed a downward-open parabolic trend. Conversely, in the scWM, FA exhibited an upward-open parabolic trajectory, while MD followed a downward-open parabolic trend. Our study demonstrates that diffusion MRI can effectively examine changes in the developing fetal cortex and confirms a prenatal onset to regional differences in cytoarchitecture that herald functional specialization.

The cellular heterogeneity of the cerebral cortex is well-documented in histological studies, and its ontogeny has been substantiated by extensive work using animal models, as well as ex vivo molecular biology analyses of human specimens (Brodmann 1909; Ding et al. 2017; Rakic 1975; Rakic 1990). Although our analysis does not incorporate tissue assays, the correspondence between changes in diffusion metrics and cellular processes can be inferred based on the timing and location of these changes. A notable observation in our study, which aligns with published data on infants born pre-term, is the high anisotropy and low diffusivity in the CP during the early second trimester (McKinstry 2002; Zhu et al. 2021). The high cellularity of the CP, along with the presence of persistent radial glial fibers from the neuronal migratory streams, impedes free water diffusion (Xu et al. 2014). As the brain matures, several factors collectively transform the CP's microenvironment, resulting in higher and more isotropic water diffusion; these factors include the regression of glial scaffolding, the cessation of neuronal migration, apoptosis of some post-migratory neurons, and the initiation of early synaptic sprouting. In the third trimester, the emergence of prominent basal dendrites from pyramidal cells and the integration of thalamocortical afferents further limit water displacement in all directions, leading to a reduction in

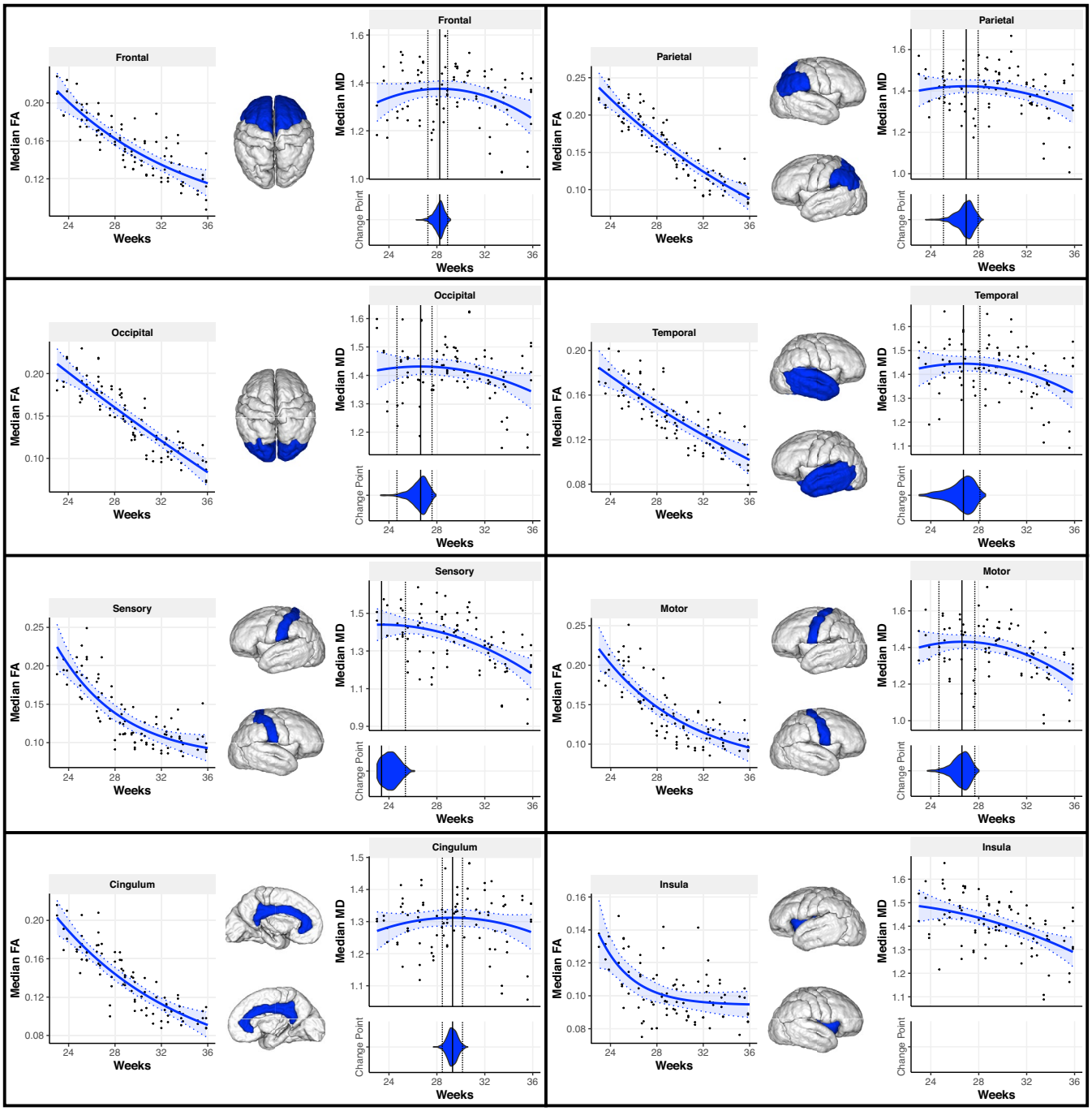

FIGURE 1 | Changes in fractional anisotropy (FA) and mean diffusivity (MD) in the corital plate between 23 and 36 weeks of gestation. A representation of each region is projected onto a surface rendering of a 35-week-old fetal brain. The panel below each MD plot corresponds to the distribution of bootstrapped samples for the vertex of the parabola. The solid vertical line corresponds to the calculated vertex, and the dotted vertical lines correspond to the 95% confidence intervals.

MD late in gestation and a subsequent decrease in FA (Huang et al. 2013). These changes are evident in our study based on the geometric changes of the diffusion tensors, as seen in Figure 4.

Our study's findings indicate that the order in which the various CP parcellations reach their peak MD aligns with anticipated synaptogenic courses (Maas et al. 2004). The sensory and motor cortex were the first to initiate this process (23.3 and 26.6 weeks, respectively), followed by the visual cortex, parietal and temporal association cortex, and finally, the prefrontal cortex (28.2 weeks). These findings are reinforced by the fact that the sensorimotor area exhibited the lowest MD at the end of gestation. On the other hand, the unique migration pathway of insular neurons and the heterogeneous laminar organization within the insula (lack of granular layer IV in some portions) may explain the differing trend observed in this region (Mallela et al. 2023).

Our findings are generally consistent with prior studies but differ in some aspects due to distinct study populations and methodologies. Ball et al. examined preterm infants between 27 and 46 weeks of GA and observed a biphasic FA pattern, with an initial decline followed by a plateau (Ball et al. 2013). Our study

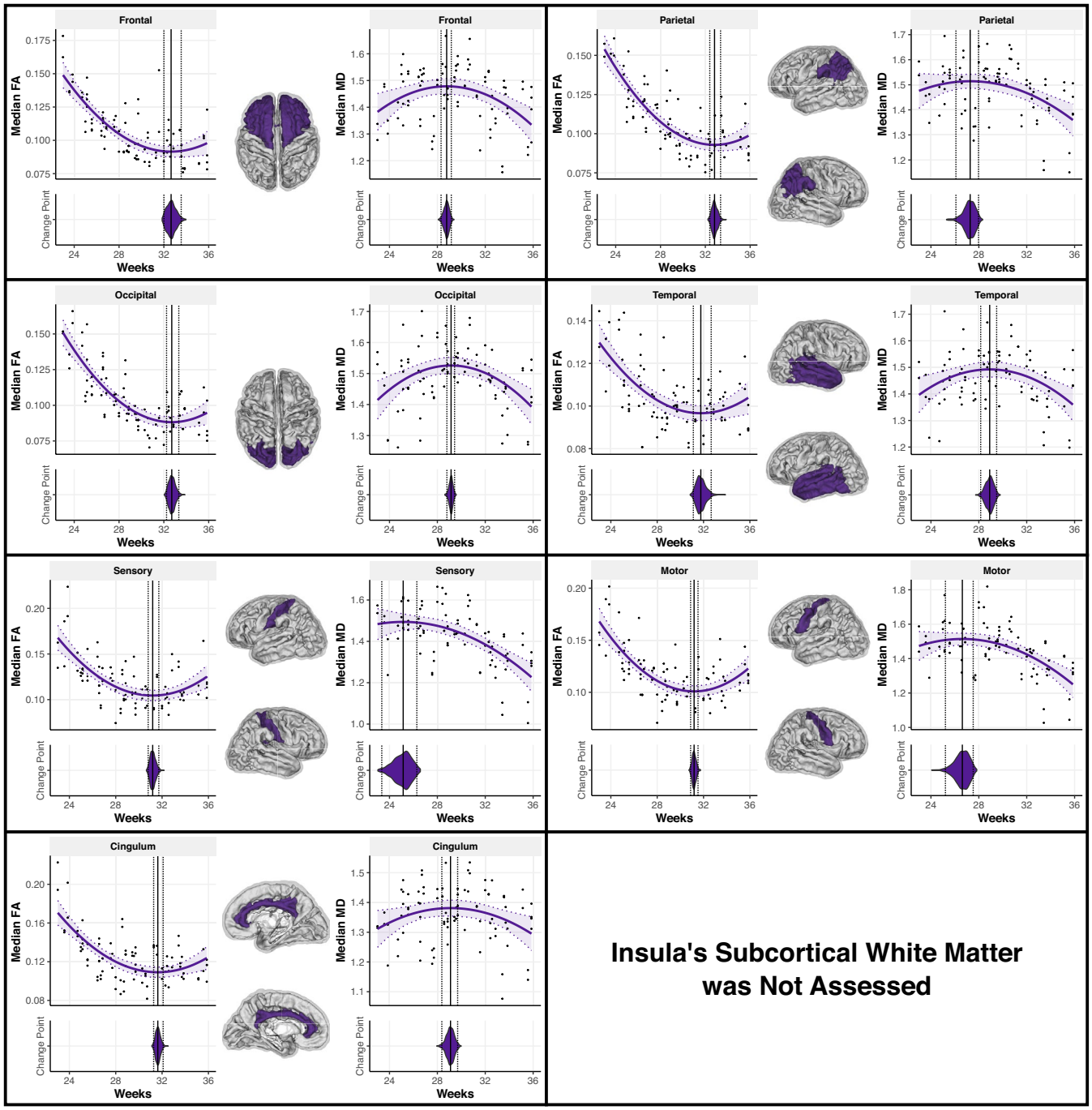

FIGURE 2 | Changes in fractional anisotropy (FA) and mean diffusivity (MD) in the subcortical white matter between 23 and 36 weeks of gestation. A representation of each region is projected onto a surface rendering of a 35-week-old fetal brain. The panel below each MD plot corresponds to the distribution of bootstrapped samples for the vertex of the parabola. The solid vertical line corresponds to the calculated vertex, and the dotted vertical lines correspond to the 95% confidence intervals.

also showed a continuous FA decline for the overlapping period (27–35 weeks), with no evidence of a flattening tail even at week 35, where FA decreased by over 20%. While Ball et al. focused on the frontal, parietal, occipital, and temporal regions, our analysis extended to additional areas, such as the insula and sensory and motor cortices, where we observed a flattened FA trajectory. The inclusion of these regions, likely contributes to some observed differences. Similarly, Ouyang et al. reported a biphasic piecewise linear FA fit, with significant declines between 31.7 and 36.4 postmenstrual weeks and stable values from 36.4 to 41.7 weeks—a period outside the scope of our study (Ouyang et al. 2019). The exponential decay model we used, which describes a process where the rate of change is initially rapid and then slows asymptotically, effectively captures this same pattern. This approach provides a simplified yet robust alternative to the biphasic models employed in earlier studies.

The changes we observed in the scWM also appear closely linked to the fetus's brain histologic changes. During the early stages of the second trimester, significant shifts in axonal organization occur, from a tortuous axonal state to a more orderly arrangement characterized by coherent axonal bundles (Dubois

TABLE 2 | Changes of diffusion metrics in the cortical plate throughout gestation.

	Cerebral zone	Description metric	Model AIC	Lateralization
Fractional anisotropy		Exponential decay constant (CI)		*p*
	Cingulum	0.13 (0.12–0.15)	−497.2516	0.62
	Frontal	0.14 (0.12–0.16)	−498.4209	0.97
	Insula	0.35 (0.25–0.49)	−504.9783	0.19
	Motor	0.16 (0.13–0.19)	−418.8283	0.05[a]
	Occipital	0.11 (0.01–0.11)	−485.2092	0.84
	Parietal	0.05 (0.01–0.11)	−447.4998	0.83
	Sensory	0.19 (0.17–0.22)	−426.7935	0.82
	Temporal	0.03 (0–0.12)	−485.9614	0.29
Mean diffusivity		Turning point in weeks (CI)		*p*
	Cingulum	29.31 (28.44–30.08)	−190.2865	0.18
	Frontal	28.24 (27.07–28.85)	−148.5962	0.78
	Insula	18.14 (−84–124.13)	−144.441	0.05[a]
	Motor	26.6 (24.7–27.6)	−110.6665	0.51
	Occipital	26.64 (24.85–27.59)	−183.8415	0.37
	Parietal	26.95 (24.95–27.88)	−155.6976	0.77
	Sensory	23.38 (18.75–25.36)	−130.9286	0.61
	Temporal	26.72 (22.38–28.12)	−131.7873	0.12

Note: Fractional anisotropy is described with an exponential decay model, while mean diffusivity is described with a quadratic model. Confidence intervals were determined using wild bootstrapping. Asymmetry was determined by calculating the laterality index and conducting a two-tailed t-test.
[a]Not significant after Holm–Bonferroni correction.

TABLE 3 | Changes of diffusion metrics in the subcortical white matter throughout gestation.

	Cerebral zone	Turning point (CI)	Model AIC	Lateralization (*p*)
Fractional anisotropy	Cingulum	31.63 (31.28–32.09)	−439.8487	0.94
	Frontal	32.65 (32.04–33.57)	−478.3092	0.52
	Motor	31.18 (30.88–31.56)	−418.8479	0.18
	Occipital	32.71 (32.22–33.35)	−500.5975	0.86
	Parietal	32.82 (32.39–33.41)	−497.076	0.36
	Sensory	31.19 (30.8–31.65)	−413.246	0.94
	Temporal	31.76 (31.15–32.71)	−493.5102	0.65
Mean diffusivity	Cingulum	29.1 (28.34–29.67)	−169.5969	0.22
	Frontal	28.78 (28.32–29.16)	−165.4805	0.44
	Motor	26.62 (25.15–27.55)	−114.7757	0.20
	Occipital	29.15 (28.83–29.42)	−186.6856	0.64
	Parietal	27.28 (26.06–28)	−162.7349	0.36
	Sensory	25.14 (23.44–26.27)	−151.5561	0.45
	Temporal	28.91 (28.13–29.51)	−145.8896	0.08

Note: Fractional anisotropy and mean diffusivity are described with a quadratic model. Confidence intervals were determined using wild bootstrapping. Asymmetry was determined by calculating the laterality index and conducting a two-tailed *t*-test. Linear regression was utilized to assess changes in the laterality index throughout gestation.

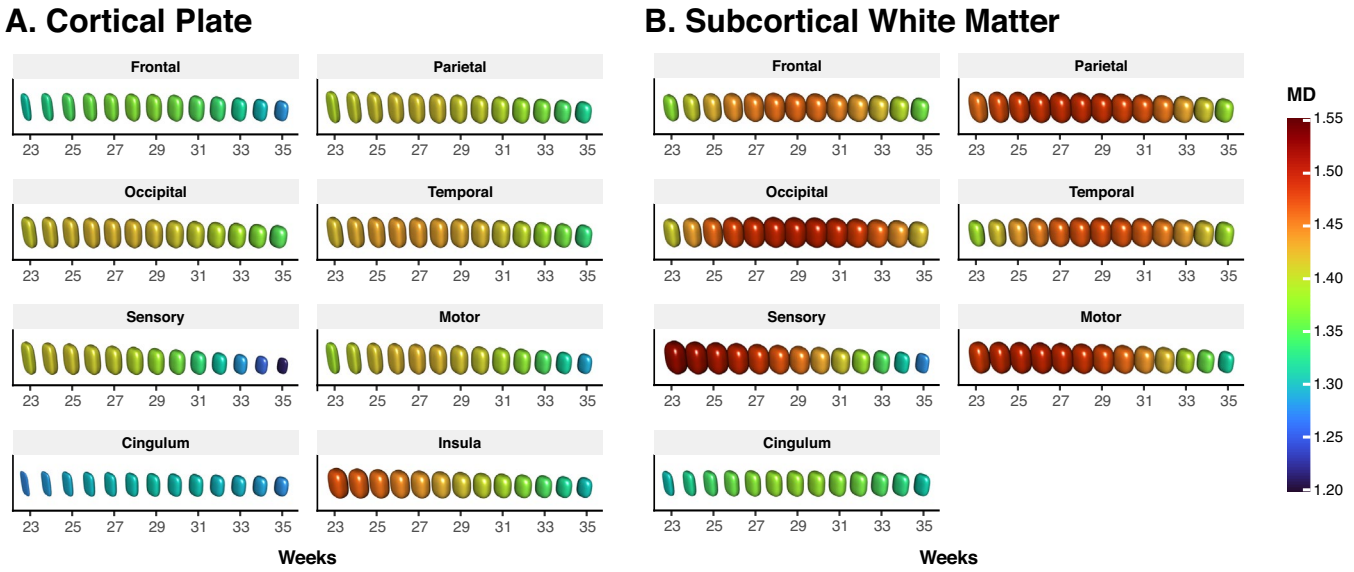

FIGURE 3 | Derivative of the estimated change rate at every point for each diffusion model in the cortical plate and subcortical white matter. The turning point for each metric is represented where the fitted line crosses 0 on the *y*-axis. The models were fitted using *z*-normalized data.

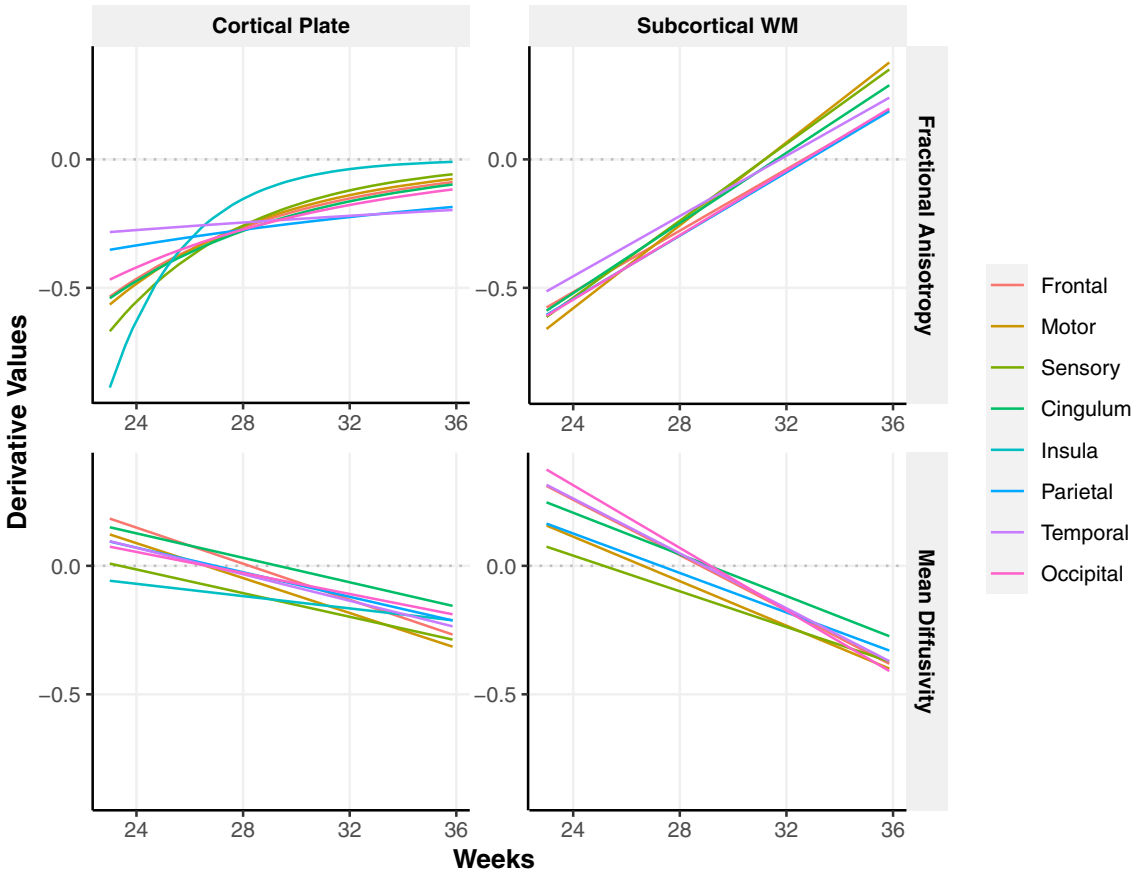

FIGURE 4 | Average diffusion tensor across gestation in each region of interest depicted using superquadric surfaces. Glyph size and color correlate directly to mean diffusivity (MD), while glyph shape conveys the anisotropy.

et al. 2008). This causes a reduction in water motion constraints, which in turn increases MD values. However, this restraint is less pronounced in the parallel direction compared to the perpendicular direction to the axons, leading to a simultaneous increase in both FA and MD values (Figure 4) (Zanin et al. 2011). It is important to note that our study sample did not show the initial increase in FA values due to the fact that it occurs in the early second trimester, whereas our study begins in the late second trimester, where initial high FA values are already present. During the later stages of gestation, immature oligodendrocytes gradually increase, and their cytoplasmic processes extend randomly (Zanin et al. 2011). This causes a reduction in water motion in all directions, leading to a decrease in FA and MD. Eventually, these cytoplasmic arborizations regress (Back

et al. 2002), and the myelin sheath progressively encircles and compacts the axons. This myelination process increases FA and further decreases MD towards the end of gestation, which is portrayed by the parabolic trends found in our study and correlates with previous studies (Calixto et al. 2023a; Jaimes et al. 2020).

Our findings demonstrate the regionally specific patterns of synchronous development of the cortical gray and associated white matter, which aligns with existing evidence. Studies have shown that intracortical white matter's myelination occurs earlier in the primary motor and sensory cortex than in other areas (Flechsig 1901; Ouyang et al. 2019). Our study supports this finding, as these regions exhibited faster decrease rates in FA and the earliest point of low FA. Additionally, our results demonstrate that the sensorimotor scWM has the highest FA at the end of gestation and the highest water diffusion restriction, as evidenced by the lowest MD at the same time.

Despite our findings, it is important to note that partial volume effects may contribute to some of the observed trends, particularly the flattening of the FA trajectory in cortical gray matter beyond 28 GW. Partial voluming is an inherent limitation of fetal diffusion MRI, especially in the context of cortical segmentation, where contributions from adjacent subcortical white matter can influence measured diffusion metrics. The degree of partial voluming likely varies across cortical regions depending on their geometry and proximity to the subplate. For example, relatively flat regions like the sensory cortex or insula may have a more uniform distribution of partial voluming between the cortical gray matter and the underlying subplate, as these surfaces have comparable volumes and adjacency. In contrast, regions with more concave geometries, such as the occipital lobe, may exhibit reduced susceptibility to partial volume effects due to the larger cortical volume and the smaller, more constrained subplate volume, which limits the proportion of voxels impacted by partial voluming. This geometric variability introduces region-specific susceptibility to partial volume effects, which may partially drive the apparent flattening of the FA trajectory in some regions (motor and sensory cortices and the insula).

Our study has several limitations. First, our sample size was limited to 44 fetuses, which can be attributed to the difficulty in recruiting normal fetuses and the moderate success rate of our pipeline. Second, the technique of fetal echo planar imaging (EPI) is known to be challenging due to its sensitivity to susceptibility artifacts, interslice motion, and signal loss, which can result in artifacts that degrade the reconstructed images. To mitigate any biases, we utilized stringent quality criteria to evaluate reconstructions and segmentations. Third, the structures of interest are located at the cusp of the spatial resolution of the acquired sequences, and there is a need for higher spatial resolution acquisition to disentangle the contributions of the different zones of the brain. Fourth, although our sample size is relatively small, it was sufficient for evaluating developmental changes over the brief period we studied. Lastly, we did not have direct histologic data to confirm the biological changes that we observed and that were driving the changes in MD and FA.

In conclusion, by utilizing a state-of-the-art computational neuroimaging framework, we identified developmental and regional differences in fetal cortical microstructure utilizing motion-corrected DTI. The changes in water diffusivity and anisotropy correlate well with known histologic changes in the late-developing fetal brain, including neuronal migration, the involution of radial glial scaffolding, and synaptic sprouting. Furthermore, this study highlights the potential for utilizing diffusion as a biomarker for normal and aberrant neurodevelopment prior to birth, at a time when most neurodiagnostic tools are unavailable (clinical exam, electroencephalography, and computed tomography) and when the interest in neuro prognostication is maximal.

Conflicts of Interest

The authors declare no conflicts of interest.

Data Availability Statement

The data that support the findings of this study are available from the corresponding author upon reasonable request.

References

Afacan, O., J. A. Estroff, E. Yang, et al. 2019. "Fetal Echoplanar Imaging: Promises and Challenges." *Top Magn Reson Imaging TMRI* 28: 245–254.

Back, S. A., N. L. Luo, N. S. Borenstein, J. J. Volpe, and H. C. Kinney. 2002. "Arrested Oligodendrocyte Lineage Progression During Human Cerebral White Matter Development: Dissociation Between the Timing of Progenitor Differentiation and Myelinogenesis." *Journal of Neuropathology and Experimental Neurology* 61: 197–211.

Ball, G., L. Pazderova, A. Chew, et al. 2015. "Thalamocortical Connectivity Predicts Cognition in Children Born Preterm." *Cereb Cortex* 25: 4310–4318.

Ball, G., L. Srinivasan, P. Aljabar, et al. 2013. "Development of Cortical Microstructure in the Preterm Human Brain." *Proceedings of the National Academy of Sciences of the United States of America* 110: 9541–9546.

Brodmann, K. 1909. *Vergleichende Lokalisationslehre der Grosshirnrinde in ihren Prinzipien dargestellt auf Grund des Zellenbaues von Dr. K. Brodmann*. J.A. Barth. https://books.google.com/books?id=Qw5KQwAACAAJ.

Calixto, C., F. Machado-Rivas, M. C. Cortes-Albornoz, et al. 2023a. "Characterizing Microstructural Development in the Fetal Brain Using Diffusion MRI From 23 to 36 Weeks of Gestation." *Cerebral Cortex* 34: bhad409.

Calixto, C., F. Machado-Rivas, D. Karimi, et al. 2023b. "Detailed Anatomic Segmentations of a Fetal Brain Diffusion Tensor Imaging Atlas Between 23 and 30 Weeks of Gestation." *Human Brain Mapping* 44: 1593–1602.

Chartier, A. L., M. J. Bouvier, D. R. McPherson, J. E. Stepenosky, D. A. Taysom, and R. M. Marks. 2019. "The Safety of Maternal and Fetal MRI at 3 T." *American Journal of Roentgenology* 213: 1170–1173.

Dikta, G., and M. Scheer. 2021. *Bootstrap Methods: With Applications in R*. Springer International Publishing. https://doi.org/10.1007/978-3-030-73480-0.

Ding, S.-L., J. J. Royall, S. M. Sunkin, et al. 2017. "Comprehensive Cellular-Resolution Atlas of the Adult Human Brain." *Journal of Comparative Neurology* 525: 407.

Dubois, J., G. Dehaene-Lambertz, M. Perrin, et al. 2008. "Asynchrony of the Early Maturation of White Matter Bundles in Healthy Infants: Quantitative Landmarks Revealed Noninvasively by Diffusion Tensor Imaging." *Human Brain Mapping* 29: 14–27.

Ennis, D. B., G. Kindlman, I. Rodriguez, P. A. Helm, and E. R. McVeigh. 2005. "Visualization of Tensor Fields Using Superquadric Glyphs." *Magnetic Resonance in Medicine* 53: 169–176.

Flechsig, P. 1901. "Developmental (Myelogenetic) Localisation of the Cerebral Cortex in the Human Subject." *Lancet* 158: 1027–1030.

Gholipour, A., J. A. Estroff, and S. K. Warfield. 2010. "Robust Super-Resolution Volume Reconstruction From Slice Acquisitions: Application to Fetal Brain MRI." *IEEE Transactions on Medical Imaging* 29: 1739–1758.

Gholipour, A., C. K. Rollins, C. Velasco-Annis, et al. 2017. "A Normative Spatiotemporal MRI Atlas of the Fetal Brain for Automatic Segmentation and Analysis of Early Brain Growth." *Scientific Reports* 7: 476.

Huang, H., T. Jeon, G. Sedmak, et al. 2013. "Coupling Diffusion Imaging With Histological and Gene Expression Analysis to Examine the Dynamics of Cortical Areas Across the Fetal Period of Human Brain Development." *Cerebral Cortex* 23: 2620–2631.

Jaimes, C., J. Delgado, M. B. Cunnane, et al. 2019. "Does 3-T Fetal MRI Induce Adverse Acoustic Effects in the Neonate? A Preliminary Study Comparing Postnatal Auditory Test Performance of Fetuses Scanned at 1.5 and 3 T." *Pediatric Radiology* 49: 37–45.

Jaimes, C., F. Machado-Rivas, O. Afacan, et al. 2020. "In Vivo Characterization of Emerging White Matter Microstructure in the Fetal Brain in the Third Trimester." *Human Brain Mapping* 41: 3177–3185.

Kainz, B., M. Steinberger, W. Wein, et al. 2015. "Fast Volume Reconstruction From Motion Corrupted Stacks of 2D Slices." *IEEE Transactions on Medical Imaging* 34: 1901–1913.

Khan, S., L. Vasung, B. Marami, et al. 2019. "Fetal Brain Growth Portrayed by a Spatiotemporal Diffusion Tensor MRI Atlas Computed From in Utero Images." *NeuroImage* 185: 593–608.

Kindlmann, G. 2004. "Superquadric Tensor Glyphs. In: Proceedings of the Sixth Joint Eurographics—IEEE TCVG Conference on Visualization. Goslar, DEU: Eurographics Association. VISSYM'04 pp 147–154."

Kuklisova-Murgasova, M., G. Quaghebeur, M. A. Rutherford, J. V. Hajnal, and J. A. Schnabel. 2012. "Reconstruction of Fetal Brain MRI With Intensity Matching and Complete Outlier Removal." *Medical Image Analysis* 16: 1550–1564.

Kunz, N., H. Zhang, L. Vasung, et al. 2014. "Assessing White Matter Microstructure of the Newborn With Multi-Shell Diffusion MRI and Biophysical Compartment Models." *NeuroImage* 96: 288–299.

Kuznetsova, A., P. B. Brockhoff, and R. H. B. Christensen. 2017. "lmerTest Package: Tests in Linear Mixed Effects Models." *Journal of Statistical Software* 82: 1–26.

Maas, L. C., P. Mukherjee, J. Carballido-Gamio, et al. 2004. "Early Laminar Organization of the Human Cerebrum Demonstrated With Diffusion Tensor Imaging in Extremely Premature Infants." *NeuroImage* 22: 1134–1140.

Machado-Rivas, F., O. Afacan, S. Khan, et al. 2021. "Spatiotemporal Changes in Diffusivity and Anisotropy in Fetal Brain Tractography." *Human Brain Mapping* 42: 5771–5784.

Mallela, A. N., H. Deng, A. Gholipour, S. K. Warfield, and E. Goldschmidt. 2023. "Heterogeneous Growth of the Insula Shapes the Human Brain." *Proceedings of the National Academy of Sciences* 120: e2220200120.

Marami, B., S. S. Mohseni Salehi, O. Afacan, et al. 2017. "Temporal Slice Registration and Robust Diffusion-Tensor Reconstruction for Improved Fetal Brain Structural Connectivity Analysis." *NeuroImage* 156: 475–488.

Marami, B., B. Scherrer, O. Afacan, B. Erem, S. K. Warfield, and A. Gholipour. 2016. "Motion-Robust Diffusion-Weighted Brain MRI Reconstruction Through Slice-Level Registration-Based Motion Tracking." *IEEE Transactions on Medical Imaging* 35: 2258–2269.

McKinstry, R. C. 2002. "Radial Organization of Developing Preterm Human Cerebral Cortex Revealed by Non-Invasive Water Diffusion Anisotropy MRI." *Cerebral Cortex* 12: 1237–1243.

Ohtaka-Maruyama, C. 2020. "Subplate Neurons as an Organizer of Mammalian Neocortical Development." *Frontiers in Neuroanatomy* 14: 8.

Ouyang, M., J. Dubois, Q. Yu, P. Mukherjee, and H. Huang. 2019. "Delineation of Early Brain Development From Fetuses to Infants With Diffusion MRI and Beyond." *NeuroImage* 185: 836–850.

Pinheiro, J., D. Bates, and R Core Team. 2023. "nlme: Linear and Nonlinear Mixed Effects Models." https://CRAN.R-project.org/package=nlme.

Pleasure, S. J., S. Anderson, R. Hevner, et al. 2000. "Cell Migration From the Ganglionic Eminences Is Required for the Development of Hippocampal GABAergic Interneurons." *Neuron* 28: 727–740.

R Core Team. 2023. *R: A Language and Environment for Statistical Computing*. R Foundation for Statistical Computing. https://www.R-project.org/.

Rakic, P. 1975. "Timing of Major Ontogenetic Events in the Visual Cortex of the Rhesus Monkey." *UCLA Forum in Medical Sciences*: 3–40.

Rakic, P. 1990. "Principles of Neural Cell Migration." *Experientia* 46: 882–891.

Rakic, P. 1995. "Radial Versus Tangential Migration of Neuronal Clones in the Developing Cerebral Cortex." *Proceedings of the National Academy of Sciences of the United States of America* 92: 11323–11327.

Taymourtash, A., H. Kebiri, E. Schwartz, et al. 2022. "Spatio-Temporal Motion Correction and Iterative Reconstruction of in-Utero Fetal fMRI." In *Medical Image Computing and Computer Assisted Intervention – MICCAI 2022*, edited by L. Wang, Q. Dou, P. T. Fletcher, S. Speidel, and S. Li, 603–612. Springer Nature Switzerland.

Trivedi, R., R. K. Gupta, N. Husain, et al. 2009. "Region-Specific Maturation of Cerebral Cortex in Human Fetal Brain: Diffusion Tensor Imaging and Histology." *Neuroradiology* 51: 567–576.

Wickham, H. 2016. *ggplot2: Elegant Graphics for Data Analysis*. Springer-Verlag New York. https://ggplot2.tidyverse.org.

Xu, G., E. Takahashi, R. D. Folkerth, et al. 2014. "Radial Coherence of Diffusion Tractography in the Cerebral White Matter of the Human Fetus: Neuroanatomic Insights." *Cerebral Cortex* 24: 579–592.

Zanin, E., J. Ranjeva, S. Confort-Gouny, et al. 2011. "White Matter Maturation of Normal Human Fetal Brain. An In Vivo Diffusion Tensor Tractography Study." *Brain and Behavior: A Cognitive Neuroscience Perspective* 1: 95–108.

Zhu, T., Q. Peng, A. Ouyang, and H. Huang. 2021. "Neuroanatomical Underpinning of Diffusion Kurtosis Measurements in the Cerebral Cortex of Healthy Macaque Brains." *Magnetic Resonance in Medicine* 85: 1895–1908.

Supporting Information

Additional supporting information can be found online in the Supporting Information section.